Supporting material for "Model for probing membrane-cortex adhesion by micropipette aspiration and fluctuation spectroscopy"

Ricard Alert[1], Jaume Casademunt[1], Jan Brugués*[2], and Pierre Sens◇[3]

[1]Departament d'Estructura i Constituents de la Matèria, Universitat de Barcelona, Avinguda Diagonal 647, 08028 Barcelona, Spain
[2]MPI of Molecular Cell Biology and Genetics, MPI for Physics of Complex Systems, Pfotenhauer Strasse 108, 01307 Dresden, Germany
[3]Laboratoire Gulliver, CNRS-ESPCI, UMR 7083, 10 rue Vauquelin, 75231 Paris Cedex 05, France. Present address: Physico-Chimie Curie, CNRS UMR 168, Institut Curie, 11 rue Pierre et Marie Curie, 75231 Paris Cedex 05, France

Contents

1 Flow dissipation in membrane displacements

In this section, the energy dissipation associated to the flows involved in the displacement of the membrane is estimated. This quantity is given by the fluid mechanics

*brugues@mpi-cbg.de
◇pierre.sens@curie.fr

of a viscous flow (1)

$$\dot{E} = 2\eta_f \int_V \vec{\vec{e}} : \vec{\vec{e}}\, dV; \qquad e_{ij} = \frac{1}{2}\left(\frac{\partial v_i}{\partial r_j} + \frac{\partial v_j}{\partial r_i}\right), \tag{1}$$

where η_f is the viscosity of the fluid flowing with a velocity field $\vec{v}$, and $\vec{\vec{e}}$ is the symmetric part of the strain rate tensor $\vec{\nabla}\vec{v}$.

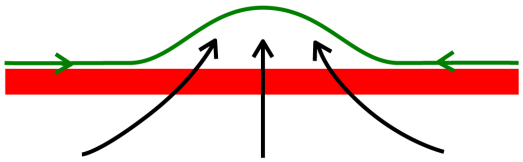

Figure 1: Sketch of membrane (green) and cytosol (black) flows involved in membrane displacements. For instance, during the initial stages of membrane-cortex detachment, i.e. bleb nucleation, the membrane is dragged over the cortex (red) and the cytosol flows through it.

There are two main sources of dissipation associated to membrane displacement, namely the lateral flow of the membrane, and the flow of cytosol through the cortex (Fig. 1). These two contributions are addressed in the two following subsections, respectively. Finally, the cytosol flow is identified as the main source of dissipation in this process. This allows to define an effective viscosity per unit length, η, characterizing the dissipative normal motion of the membrane as in Eq. 1 in the Main Text.

1.1 Membrane flow dissipation

We start by considering the lateral flow of the membrane respect to the underlying cortex. Suppose that the membrane is flowing towards a membrane patch that is inflating. This patch can be thought of as a nucleating bleb of circular projected area of radius a. The increase of the membrane area of this incipient bleb per unit time, $\dot{S}_b$, is given by membrane mass conservation: $\dot{S}_b = 2\pi r\dot{r}$, where r is the distance from any point along the membrane to the center of the bleb (cylindrical coordinates), and $\dot{r}$ is the radial flow speed (Fig. 2).

However, the flowing speed of the membrane must vanish at the points at which it is connected to the cortex through linker molecules. This gives rise to a local velocity gradient of order $\dot{r}/\xi_0 = \dot{S}_b/\left(2\pi r\xi_0\right)$ between any two linkers, with $\rho_0 \equiv \xi_0^{-2}$ the density of linkers. In turn, the global radial velocity gradient of membrane flow is of order $\dot{r}/r = \dot{S}_b/\left(2\pi r^2\right)$. Therefore, the total membrane flow dissipation $\dot{E}_m$ will include the contributions of these two gradients: $\dot{E}_m = \dot{E}_m^{\text{links}} + \dot{E}_m^{\text{global}}$. Then, based on Eq. 1, these are estimated by

$$\dot{E}_m^{\text{links}} \sim 4\pi\eta_m g \int_a^R r dr \left(\frac{\dot{S}_b}{2\pi r\xi_0}\right)^2 = \frac{\eta_m g \dot{S}_b^2}{\pi\xi_0^2} \ln\left(\frac{R}{a}\right) \approx \frac{\eta_m g \dot{S}_b^2}{2\pi\xi_0^2} \ln\left(\frac{S}{4A_b}\right), \tag{2}$$

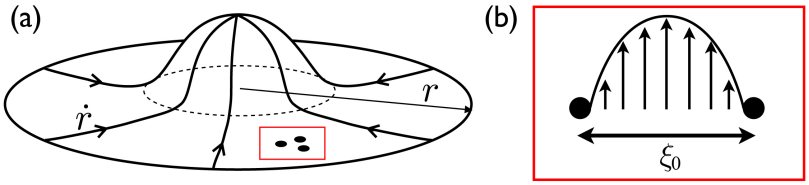

Figure 2: Membrane flow dissipation. (a) Sketch of the membrane flow towards a given patch (dotted line). (b) This flow vanishes at the position of the membrane-cortex linkers (black dots), which results in a gradient of the flow velocity.

$$\dot{E}_m^{\text{global}} \sim 4\pi\eta_m g \int_a^R r dr \left(\frac{\dot{S}_b}{2\pi r^2}\right)^2 \approx \frac{\eta_m g \dot{S}_b^2}{2\pi a^2} = \frac{\eta_m g \dot{S}_b^2}{2A_b}. \tag{3}$$

Here, η_m is the viscosity of the membrane, g its thickness, and R is the cell radius. Accordingly, $S = 4\pi R^2$ is the total visible area of the cell membrane, and $A_b = \pi a^2$ is the projected circular area of the incipient bleb. Our continuum approach describes membrane displacements at length scales larger than ξ_0^2. As a consequence, $A_b > \pi\xi_0^2$ and the local dissipation between linkers, $\dot{E}_m^{\text{links}}$, is expected to dominate membrane flow dissipation.

1.2 Cytosol flow dissipation

Next we compute the energy dissipation rate due to the flow of the cytosol during membrane displacements. In the incompressible regime of cytosol flow, mass conservation reads $\dot{V}_b = 4\pi\varrho^2 v_\varrho$, where V_b is the volume of the incipient bleb, ϱ is now the distance from any point in the cytoplasm to the tip of the bleb (spherical coordinates), and v_ϱ is the fluid velocity at this point. As for the membrane flow, there are two velocity gradients contributing to dissipation; in this case: $\dot{E}_c = \dot{E}_c^{\text{cortex}} + \dot{E}_c^{\text{global}}$. The first one corresponds to the flow of the cytosol through the cortex, which generates velocity gradients of order $v_\varrho/\xi = \dot{V}_b/\left(4\pi\varrho^2\xi\right)$ only inside the cortex. The second one corresponds to the global radial velocity gradient of order $v_\varrho/\varrho = \dot{V}_b/\left(4\pi\varrho^3\right)$ spanning throughout the cytoplasm.

The computation of the cortex term can be done by considering the cortex as a porous material. In this sense, the cortex is viewed as an array of thin capillary tubes of typical radius ξ, so that cylindrical coordinates are the most appropriate in this case. We also consider that the flow of the cytosol through the cortex is along the axial coordinate z and is restricted to the cortical area where the bleb is nucleating (Fig. 1), i.e. a circular area of radius a. Therefore, the number of capillary tubes involved in the cytosol flow through the cortex is $\sim a^2/\xi^2$, so that the total dissipation is this number times the dissipation along one tube. In turn, the cortex is considered to be separated a distance $\sim a$ from the tip of the incipient bleb, so that it is located at $a < z < a + h$, where h is its thickness. Then, using Eq. 1 as before:

$$\dot{E}_c^{\text{cortex}} \sim \frac{a^2}{\xi^2} 4\pi\eta_c \int_a^{a+h} dz \int_0^{\xi} r dr \left(\frac{\dot{V}_b}{4\pi z^2 \xi}\right)^2 \approx \frac{\eta_c h \dot{V}_b^2}{4\pi\xi^2 a^2} = \frac{\eta_c h \dot{V}_b^2}{4\xi^2 A_b}, \tag{4}$$

where we have used $h < a$ to obtain an approximate expression valid for the large length-scale motion that our model describes.

Finally, the global term is dealt with using spherical coordinates in Eq. 1:

$$\dot{E}_c^{\text{global}} \sim 8\pi\eta_c \int_a^R \varrho^2 d\varrho \left(\frac{\dot{V}_b}{4\pi\varrho^3}\right)^2 \approx \frac{\eta_c \dot{V}_b^2}{6\pi a^3} = \frac{\sqrt{\pi}\,\eta_c \dot{V}_b^2}{6A_b^{3/2}}. \tag{5}$$

Similar to the case of the membrane dissipation, since $A_b > \pi\xi^2$, the contribution of the permeation through the cortex is expected to dominate the dissipation associated to cytosol flow.

1.3 Effective viscosity of membrane displacements

In conclusion, an estimate for the rate of energy dissipation due to the flows involved in sufficiently extended membrane displacements is given by

$$\dot{E} \sim \dot{E}_m^{\text{links}} + \dot{E}_c^{\text{cortex}} \sim \frac{\eta_m g \dot{S}_b^2}{2\pi\xi_0^2} \ln\left(\frac{S}{4A_b}\right) + \frac{\eta_c h \dot{V}_b^2}{4\xi^2 A_b}, \tag{6}$$

where only the relevant contributions of the membrane and cytosol flows have been included. Next, $\dot{S}_b$ and $\dot{V}_b$ need to be estimated in terms of membrane displacement u and speed $\dot{u}$. This can be done by considering the shape of the incipient bleb as a spherical cap of radius R_b, polar radius a, and height u. Then,

$$S_b \sim 2\pi R_b u, \qquad V_b \sim \pi R_b u^2; \qquad R_b = \frac{1}{2}\left(\frac{a^2}{u} + u\right). \tag{7}$$

The polar radius a is assumed to remain constant during the inflation of the bleb, while both u and R_b change. Then, the previous expressions need to be rewritten in terms of a single dynamical variable, namely u:

$$S_b \sim \pi\left(a^2 + u^2\right), \qquad V_b \sim \frac{\pi a^2}{2} u \tag{8}$$

to the lowest order in the height u. Now, if the bleb is inflating at a speed $\dot{u}$,

$$\dot{S}_b \sim 2\pi u \dot{u}, \qquad \dot{V}_b \sim \frac{\pi a^2}{2}\dot{u}. \tag{9}$$

According to Eq. 6, this means that the main contribution to dissipation is the flow of cytosol through the cortex for small enough membrane displacements u, to which our linear model is restricted:

$$\dot{E} \sim \frac{\eta_c h A_b}{4\xi^2}\dot{u}^2. \tag{10}$$

This allows to define $\mu_{\text{eff}} \sim \eta_c h A_b/\xi^2$ as the effective drag coefficient for the overdamped motion of the membrane: $F = \mu_{\text{eff}}\dot{u}$. Then, when the dynamics of uniform membrane displacements is specified per unit area, Eq. 1 in the Main Text is retrieved together with the mentioned definition of the effective viscosity per unit length η, given by:

$$\eta \equiv \frac{\mu_{\text{eff}}}{A_b} \sim \eta_c \frac{h}{\xi^2}. \tag{11}$$

It is worth remarking that the overdamped limit for membrane dynamics has been argued to be valid in (2).

2 Membrane undulations

2.1 Adhesion-induced correlations

Under the adiabatic approximation, and at length scales larger than $\rho_0^{-1/2}$, membrane dynamics is fully described in terms of the dispersion relation

$$\omega(q) = -\frac{\kappa q^4 + \gamma q^2 + \rho_{b,\mathrm{eq}} k}{4\eta_c q}, \tag{12}$$

as given by Eq. 15 in the Main Text. Because of membrane-cortex adhesion, the dispersion relation features a maximum at a finite wavelength. Fig. 3 shows that the nonmonotonic behaviour of the dispersion relation is associated to adhesion, disappearing in its absence ($\rho_{b,\mathrm{eq}} = 0$). Indeed, membrane-cortex adhesion is also responsible for the divergence of the dispersion relation at large wavelengths, which disappears if the hydrodynamic effects of the cortex are accounted for (see section 4).

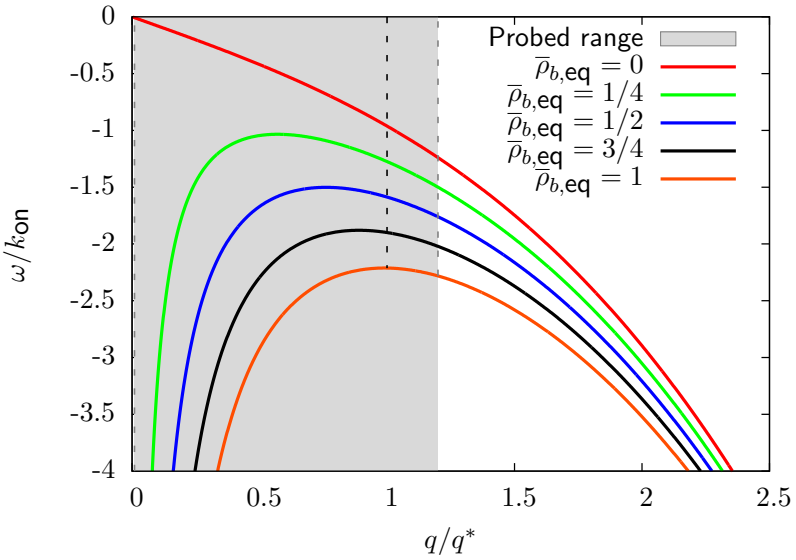

Figure 3: Growth rate of a membrane undulation of wave-vector q for different values of the fraction of bound linkers $\overline{\rho}_{b,\mathrm{eq}} = \rho_{b,\mathrm{eq}}/\rho_0$. The rescaling wave-vector is defined as $q^* = 2\pi/\lambda^*$ with $\lambda^* \equiv \lambda_c(\rho_0)$. The range of wave-vectors experimentally explored in (3) is shaded in grey. This indicates that the non-monotonicity of the dispersion relation due to membrane-cortex adhesion could be probed in fluctuation spectroscopy experiments

The finite wavelength $\lambda_c(\rho_{b,\mathrm{eq}})$ at which the growth rate $\omega(q)$ is maximum, gives the length scale of membrane deformations that feature the slowest relaxation. Consequently, this wavelength acts as a correlation length of membrane undulations.

2.2 Membrane structure factor

Under the adiabatic approximation, and at length scales larger than $\rho_0^{-1/2}$, the structure factor of membrane fluctuations reads

$$S(q) = \frac{k_B T}{\kappa q^4 + \gamma q^2 + \rho_{b,\mathrm{eq}} k}, \tag{13}$$

as given in Eq. 17 of the Main Text. Fig. 4 plots the dependence of the structure factor on the wave-vector q, showing that long-wavelength undulations are the most prominent in terms of amplitude. This fact reinforces the picture of the adhered membrane as a rigid-like object at short scales, with no relevant contribution of undulations. In particular, Fig. 4b shows that fluctuations of length scale smaller than λ^* are not associated to an increase of stress of the linkers, and this should not contribute to setting the location of the unbinding transition. Hence, this explains the role of λ^* as a correlation length separating the rigid-like and undulated regimes of the membrane.

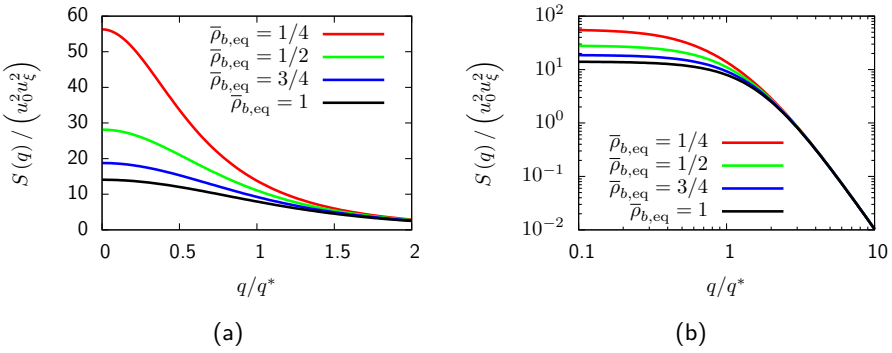

Figure 4: Membrane structure factor as a function of the wave-vector for different values of the fraction of bound linkers $\overline{\rho}_{b,\mathrm{eq}} = \rho_{b,\mathrm{eq}}/\rho_0$. The rescaling lengths are $u_0 \equiv k_B T/(k\delta)$ and $u_\xi \equiv k_B T/(k\xi)$. (a) In linear scale. (b) In logarithmic scale, which evidences the crossover between the regime where adhesion dominates ($\lambda^* q < 1$), and the regime where membrane mechanics dominates ($\lambda^* q > 1$).

2.3 Amplitude of membrane undulations

The mean-square amplitude of membrane undulations can be obtained by Fourier-transforming the membrane structure factor Eq. 13 back to real space:

$$\left\langle \delta u^2(\vec{x}) \right\rangle = \frac{k_B T}{2\pi} \frac{1}{\sqrt{4\kappa\rho_{b,\mathrm{eq}} k - \gamma^2}} \left[\arctan\left(\frac{2\pi^2 \kappa \rho_0 + \gamma}{\sqrt{4\kappa\rho_{b,\mathrm{eq}} k - \gamma^2}} \right) - \arctan\left(\frac{2\kappa (\pi/L)^2 + \gamma}{\sqrt{4\kappa\rho_{b,\mathrm{eq}} k - \gamma^2}} \right) \right]. \tag{14}$$

This is the result for the case $\gamma^2 < 4\kappa\rho_{b,\mathrm{eq}} k$, which is the actual situation for our choice of $k \sim 10^{-4}$ N/m. Next, some limits of Eq. 14 are studied:

- Strong adhesion:

$$\lim_{\rho_{b,\mathrm{eq}}k\to\infty}\left\langle \delta u^2\left(\vec{x}\right)\right\rangle \approx \frac{k_BT\pi\rho_0}{4\rho_{b,\mathrm{eq}}k}, \tag{15}$$

  which does not diverge for large membranes due to adhesion. It corresponds to a rigid and unstretchable membrane fluctuating under the harmonic confinement of the average adhesion potential $\rho_{b,\mathrm{eq}}k$ acting down to the cutoff length $\rho_0^{-1/2}$.

- Low tension:

$$\lim_{\gamma\to 0}\left\langle \delta u^2\left(\vec{x}\right)\right\rangle \approx \frac{k_BT}{8\sqrt{\kappa\rho_{b,\mathrm{eq}}k}}, \tag{16}$$

  which does not diverge either. This situation corresponds, for instance, to the case of a somehow constrained vesicle, where membrane surface tension is negligible as compared to bending rigidity. A constraining harmonic confinement, which can stem from other membranes in a stack (4), the presence of a nearby wall (5), or sparse harmonic attachments (6), produces the same effect as the adhesion term within the adiabatic approximation framework of our model.

- High bending rigidity:

$$\lim_{\kappa\to\infty}\left\langle \delta u^2\left(\vec{x}\right)\right\rangle \approx \frac{k_BTL^2}{4\pi^3\kappa}. \tag{17}$$

  In this case, the root mean-square amplitude diverges linearly with the membrane linear size. This limit corresponds to a free vesicle in the absence of any adhesion or confinement, so that undulations are driven solely by bending rigidity (7).

It is worth exploring the other possible case, namely $\gamma^2 > 4\kappa\rho_{b,\mathrm{eq}}k$, since it could be relevant for some cell types, for instance, presenting a more diluted cortex or softer linkers. In this case, the mean-square amplitude of membrane undulations reads

$$\left\langle \delta u^2\left(\vec{x}\right)\right\rangle = \frac{k_BT}{4\pi}\frac{1}{\sqrt{\gamma^2-4\kappa\rho_{b,\mathrm{eq}}k}}\left[\ln\left(\frac{2\pi^2\kappa\rho_0+\gamma-\sqrt{\gamma^2-4\kappa\rho_{b,\mathrm{eq}}k}}{2\pi^2\kappa\rho_0+\gamma+\sqrt{\gamma^2-4\kappa\rho_{b,\mathrm{eq}}k}}\right)-\right.$$
$$\left.\ln\left(\frac{2\kappa\left(\pi/L\right)^2+\gamma-\sqrt{\gamma^2-4\kappa\rho_{b,\mathrm{eq}}k}}{2\kappa\left(\pi/L\right)^2+\gamma+\sqrt{\gamma^2-4\kappa\rho_{b,\mathrm{eq}}k}}\right)\right]. \tag{18}$$

The limits for this situation are discussed below:

- Weak adhesion:

$$\lim_{\rho_{b,\mathrm{eq}}k\to 0}\left\langle \delta u^2\left(\vec{x}\right)\right\rangle \approx \frac{k_BT}{2\pi\gamma}\ln\left(\frac{L}{\pi}\sqrt{\frac{\gamma}{\kappa}}\right), \tag{19}$$

  which diverges logarithmically for large membranes. This corresponds to the case of a free membrane with contributions both of bending and surface tension to undulations.

- High tension:

$$\lim_{\gamma\to\infty}\left\langle \delta u^2\left(\vec{x}\right)\right\rangle \approx \frac{k_B T}{2\pi\gamma}\ln\left(\rho_0^{1/2}L\right), \tag{20}$$

which also diverges logarithmically for large membranes. This is the result obtained in the absece of adhesion for tension-dominated membrane dynamics (8). This situation might correspond to a strongly stretched membrane due to cortical pulling.

- Low bending rigidity:

$$\lim_{\kappa\to 0}\left\langle \delta u^2\left(\vec{x}\right)\right\rangle \approx \frac{k_B T}{4\pi\gamma}\ln\left(1+\frac{\pi^2\gamma\rho_0}{\rho_{b,\mathsf{eq}}k}\right), \tag{21}$$

which does not diverge for large membranes due to adhesion. This situation corresponds to a very flexible membrane yet under tension, and adherent.

$\gamma^2 < 4\kappa\rho_{b,\mathsf{eq}}k$	no limit	~ 3 nm
	$\rho_{b,\mathsf{eq}}k \to \infty$	~ 6 nm
	$\gamma \to 0$	~ 4 nm
	$\kappa \to \infty$	~ 1 μm
$\gamma^2 > 4\kappa\rho_{b,\mathsf{eq}}k$	no limit	—
	$\rho_{b,\mathsf{eq}}k \to 0$	~ 9 nm
	$\gamma \to \infty$	~ 9 nm
	$\kappa \to 0$	~ 3 nm

Table 1: Numerical estimates for the root mean-square amplitude of membrane undulations $\left\langle \delta u^2\left(\vec{x}\right)\right\rangle^{1/2}$ in different situations and limits. In all cases, the same numerical values of the parameters have been used.

Table 1 summarizes the numerical values of the root mean-square amplitude of membrane undulations for all the cases and limits discussed above. The value $\left\langle \delta u^2\left(\vec{x}\right)\right\rangle^{1/2} \sim 3$ nm corresponding to our case justifies the approximation of considering the membrane-cortex linker molecules as hookean springs, i.e. in their linear elasticity regime.

2.4 Membrane power spectrum

Within the adiabatic approximation, the power spectrum reads

$$S\left(\omega\right) = \frac{4\eta_c k_B T}{\pi}\int_{q_{\mathsf{min}}}^{q_{\mathsf{max}}} \frac{dq}{\left(4\eta_c\omega\right)^2 + \left(\kappa q^3 + \gamma q + \rho_{b,\mathsf{eq}}k/q\right)^2}, \tag{22}$$

as given by Eq. 19 in the Main Text. This expression can not be analytically integrated in general. Next we consider some asymptotic behaviours of this expression. Integration limits are extended to $q_{\mathsf{min}} \to 0$ and $q_{\mathsf{max}} \to \infty$ whenever possible:

- No adhesion. Tension-dominated regime, low frequencies: Low-frequency responses of a non-adhered membrane are found at long wavelengths, and are thus dominated by surface tension: $\lim_{q\to 0}\omega\left(q\right) = \gamma q/\left(4\eta_c\right)$. Therefore,

the low-frequency limit of the power spectrum of a free membrane can be retrieved by imposing a vanishing bending rigidity $\kappa \to 0$:

$$\lim_{\kappa \to 0} S(\omega) = \frac{k_B T}{2\gamma\omega}. \tag{23}$$

- No adhesion. Bending-dominated regime, high frequencies: High relaxation rates of the free membrane occur at $q \to \infty$, implying that they are dominated by the bending rigidity: $\lim_{q\to\infty} \omega(q) = \kappa q^3/(4\eta_c)$. Consequently, the high-frequency limit of the power spectrum of a non-adhered membrane is retrieved by neglecting surface tension $\gamma \to 0$:

$$\lim_{\gamma \to 0} S(\omega) = \frac{k_B T}{6\left(2\kappa\eta_c^2\right)^{1/3}\omega^{5/3}}. \tag{24}$$

- Adhesion-dominated regime, intermediate-high frequencies: As opposed to the behaviour of free membranes, the dispersion relation of a membrane adhered to the cortex in the adiabatic approximation is non-monotonic. Therefore, the relationship between frequencies and wave-vectors is not straightforward. For the range of wave-vectors experimentally explored in (3), with $d_f = 0.5$ μm, we have $\omega(q_{\mathsf{min}}) \gg \omega(q_{\mathsf{max}})$, as shown in Fig. 3. Consequently, the adhesion-dominated regime at long wavelengths corresponds to high frequencies. Using smaller focal light spots could shift the adhesion-dominated regime towards lower frequencies. An analytical expression for the power spectrum in this limit is worked out by setting $\kappa, \gamma \to 0$:

$$\lim_{\kappa,\gamma \to 0} S(\omega) = \frac{k_B T}{4\pi\eta_c\omega^2}\left[q_{\mathsf{max}} - q_{\mathsf{min}} + \right.$$
$$\left. + \frac{\rho_{b,\mathsf{eq}} k}{4\eta_c\omega}\left[\arctan\left(\frac{4\eta_c q_{\mathsf{min}}\omega}{\rho_{b,\mathsf{eq}} k}\right) - \arctan\left(\frac{4\eta_c q_{\mathsf{max}}\omega}{\rho_{b,\mathsf{eq}} k}\right)\right]\right]. \tag{25}$$

- Brownian motion regime, highest frequencies: Finally, at sufficiently high frequencies the power spectrum is only revealing the Brownian motion of the membrane within the cytosol, which only depends on the viscosity of the latter. This limit is thus insensitive to any membrane properties:

$$\lim_{\omega \to \infty} S(\omega) = \frac{k_B T\left(q_{\mathsf{max}} - q_{\mathsf{min}}\right)}{4\pi\eta_c\omega^2}. \tag{26}$$

On the one hand, the first two limits correspond to a non-adhered membrane, for which our model retrieves the predicted (9) and observed (3, 9, 10) scalings $\sim \omega^{-1}$ and $\sim \omega^{-5/3}$ of the power spectrum. These studies also predicted and observed the high-frequency $\sim \omega^{-2}$ behaviour corresponding to the Brownian motion of the membrane within the surrounding fluid. Finally, if the effect of the hydrodynamic confinement due to the presence of the cortex is important, which turns out to be the case for red blood cells, one should expect an intermediate regime scaling as $\sim \omega^{-4/3}$ (11).

3 Validity of the flat-membrane model

Here we analyze the validity of the flat-membrane model as a function of membrane-cortex adhesion. On the one hand, Fig. 5a plots the dependence of the correlation length λ_c on the density of bonds (Eq. 16 of the Main Text), evindencing the increased membrane correlations near the unbinding transition. As a consequence, the simple flat-membrane model becomes more accurate near detachment. On the other hand, Fig. 5b shows the increase in the amplitud of membrane fluctuations (Eq. 14) when membrane-cortex adhesion is weakened, specially at long-wavelength (see also Fig. 4). The magnification of membrane undulations near the unbinding transition implies that a stochastic version of the adhesion models presented in this article may be needed for an accurate study of membrane-cortex detachment.

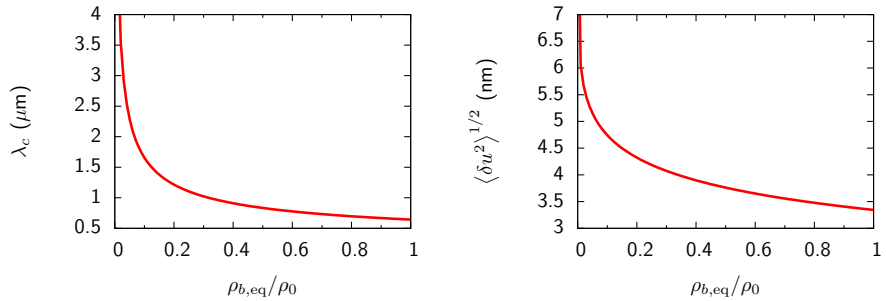

(a) (b)

Figure 5: Membrane correlations and undulations as a function of adhesion. (a) Correlation length of membrane undulations as a function of the equilibrium density of bonds. (b) Root mean-square amplitude of membrane undulations as a function of the equilibrium density of bonds.

4 Influence of a nearby porous cortex on membrane dynamics

Here we comment on the effects of the cortex over the hydrodynamics of the membrane. Under the adiabatic approximation, membrane-cortex adhesion acts as an effective harmonic confining potential of stiffness $\rho_{b,\mathrm{eq}}k$. For a harmonically confined membrane, the presence of a nearby porous wall has been shown to modify the dispersion relation by a mode-dependent factor (5):

$$\omega\left(q\right)=\omega_0\left(q\right)e^{-2Dq}\frac{e^{2Dq}\left(1+4L_pq\right)-1-2Dq-2\left(Dq\right)^2\left(1+2L_pq\right)}{1+4L_pq}, \quad (27)$$

where D is the distance between the membrane and the cortex, and L_p is the cortical permeation length. The latter is defined as $L_p=\sqrt{\eta_c\left(1-\phi_v\right)K_p}$, where η_c is the viscosity of the cytosol, ϕ_v is the volume fraction of the cortex, and K_p is its volume permeability (12). Finally, $\omega_0\left(q\right)$ is the dispersion relation in the absence

of hydrodynamic effects due to the cortex:

$$\omega_0(q) = -\frac{\kappa q^4 + \gamma q^2 + \rho_{b,\mathrm{eq}} k}{4\eta_c q}. \tag{28}$$

Fig. 6 plots the modified relaxation rates for different values of the membrane-cortex distance D and the cortical permeation length L_p. The inclusion of the cortex in the hydrodynamics introduces a cutoff of the relaxation rate at low wave-vectors, in contrast to the divergence shown in Fig. 3. This is the only qualitative change on the dispersion relation arising from the influence of the cortex when it is either far from the membrane or porous enough. In this case, $\omega(q)$ still displays a (possibly local) minimum defining a correlation length. The position of this minimum is slightly shifted, now appearing at longer wavelengths, so that the correlation length of membrane undulations increases from $\lambda^* \sim 0.6$ μm. This would reinforce the adiabatic approximation as well as widen the range of validity of the simple flat-membrane model.

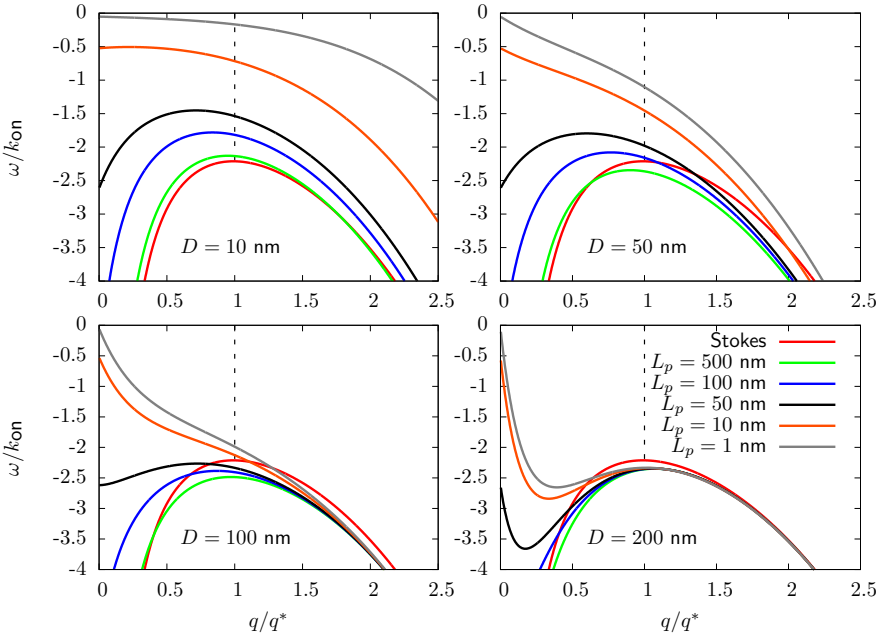

Figure 6: Growth rate of a membrane undulation of wave-vector q for $\rho_{b,\mathrm{eq}} = 1$ and for different values of the membrane-cortex distance D and cortical permeation length L_p. The curve in the absence of cortical influence on membrane hydrodynamics (Stokes) is always shown for comparison.

In turn, low membrane-cortex distances or less permeable cortices would have a stronger influence on membrane hydrodynamics and produce deeper modifications of the dispersion relation. In some cases, the dispersion relation would not even have a local minimum and, therefore, no finite correlation length could be defined. However, this would not invalidate the main conclusions drawn from the analysis of membrane undulations, namely the fact that the flat-membrane model is restricted

to short length scales for large-amplitude undulations, and the possibility to extract the density of bound linkers from fluctuation spectroscopy experiments. Concerning the first one, the lack of a correlation length would simply imply that the crossover length scale below which the flat-membrane model applies could not be estimated a priori. For the second conclusion, the density of bound linkers $\rho_{b,\mathrm{eq}}$ would still be obtainable from the experimental structure factor $S(q)$ or power spectrum $S(\omega)$ but the theoretical fitting curves would not be given by Eq. 13, and Eq. 25, respectively, anymore and they would demand knowledge of D and L_p, instead.

References

1. Guyon, E., J.-P. Hulin, L. Petit, and C. D. Mitescu. 2001. Physical hydrodynamics. Oxford University Press.

2. Lin, L. and F. Brown. 2005. Dynamic simulations of membranes with cytoskeletal interactions. *Phys. Rev. E.* 72:011910.

3. Betz, T. and C. Sykes. 2012. Time resolved membrane fluctuation spectroscopy. *Soft Matter* 8:5317.

4. de Gennes, P. G. and C. Taupin. 1982. Microemulsions and the flexibility of oil/water interfaces. *J. Phys. Chem.* 86:2294–2304.

5. Gov, N., , A. Zilman, and S. Safran. 2004. Hydrodynamics of confined membranes. *Phys. Rev. E.* 70:011104.

6. Gov, N. and S. Safran. 2004. Pinning of fluid membranes by periodic harmonic potentials. *Phys. Rev. E.* 69:011101.

7. Boal, D. 2002. Mechanics of the cell. Cambridge University Press.

8. Safran, S. A. 1994. Statistical thermodynamics of surfaces, interfaces, and membranes. Addison-Wesley.

9. Helfer, E., S. Harlepp, L. Bourdieu, J. Robert, F. MacKintosh, and D. Chatenay. 2001. Viscoelastic properties of actin-coated membranes. *Phys. Rev. E.* 63:021904.

10. Betz, T., M. Lenz, J.-F. Joanny, and C. Sykes. 2009. ATP-dependent mechanics of red blood cells. *Proc. Natl. Acad. Sci. USA.* 106:15320–5.

11. Gov, N. S., A. G. Zilman, and S. A. Safran. 2003. Cytoskeleton confinement and tension of red blood cell membranes. *Phys. Rev. Lett.* 90:228101.

12. Ranft, J., J. Prost, F. Jülicher, and J.-F. Joanny. 2012. Tissue dynamics with permeation. *Eur. Phys. J. E.* 35:46.